Supporting Information

$CaCO_3$-based carriers with prolonged release property for antifungal drug delivery to hair follicles

Mariia S. Saveleva[a], Ekaterina V. Lengert[a], Roman A Verkhovskii[a], Anatolii A. Abalymov[a], Anton M. Pavlov[b], Alexey V. Ermakov[a,c], Ekaterina S. Prikhozhdenko[a], Sergei N. Shtykov[d], Yulia I. Svenskaya[a*]

[a]Science Medical Center, Saratov State University, 410012 Saratov, Russia

[b]Research and Educational Institute of Nanostructures and Biosystems, Saratov State University, 410012 Saratov, Russia

[c]First Moscow State Medical University (Sechenov University), Moscow 119992, Russia

[d]Department of Analytical Chemistry and Chemical Ecology, Saratov State University, 410012 Saratov, Russia

*Corresponding author: Yulia Svenskaya, e-mail: svenskaya@info.sgu.ru

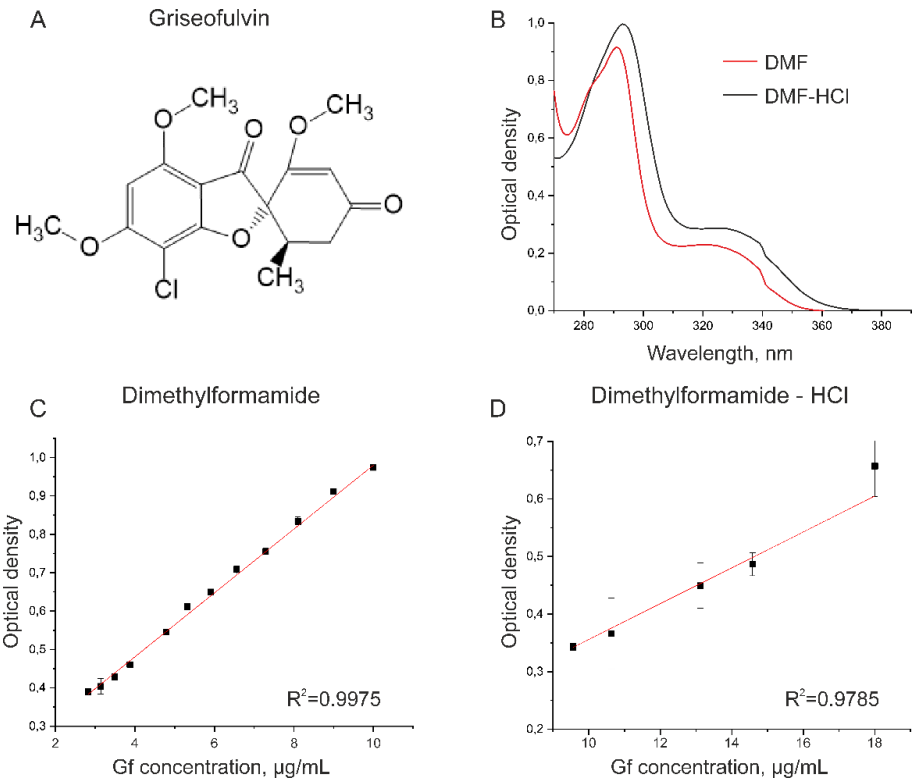

Figure SI 1. (**A**) - structural formula of griseofulvin (Gf); (**B**) - the absorption spectra of Gf in dimethylformamide (DMF) and DMF-HCl mixture (1:1 ratio), Gf concentration is 9 and 18 µg/mL. respectively; (**C**) and (**D**) – calibration curves of Gf in DMF and DMF-HCl mixture (1:1 ratio) correspondingly. The data in (C, E) are presented as a "mean value ± standard error".

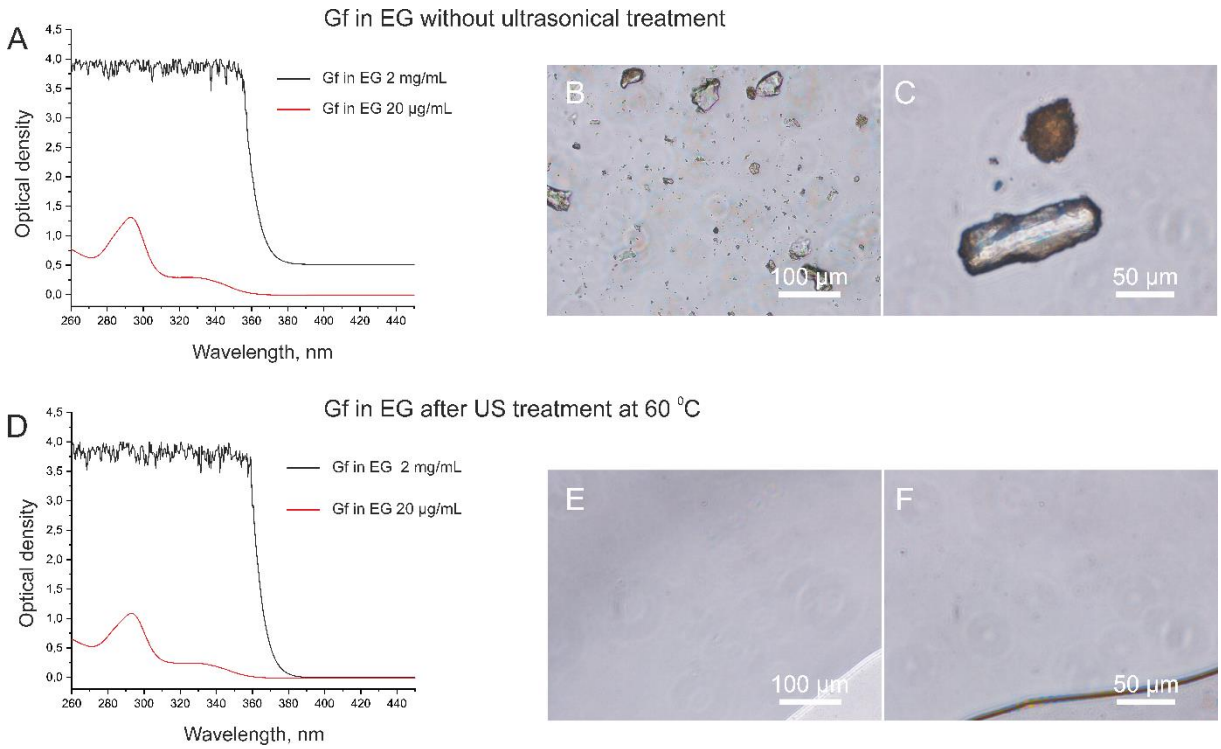

Figure SI 2. The absorption spectra of the griseofulvin (Gf) in ethylene glycol (EG) dissolved under various conditions: (**A**) – the dissolution process was performed without any physical treatment; (**D**) - the dissolution process was performed with simultaneous sonication and heating (60 ^{o}C) during 1 hour with an ultrasonic bath. The images represent spectra of 2 mg/mL Gf solutions obtained at these conditions (black lines) and 100 times diluted ones (red lines). The non-zero baseline in image A indicates limited solubility of Gf in EG and, thus, presence of sediment in the 2 mg/mL suspension when no additional treatment is applied. Optical microscopy images (**B, C**) confirmed the presence of Gf particles in this suspension. Meanwhile, treatment of such suspension with an ultrasonic bath allowed for the Gf solubility enhancement resulting in its complete dissolution in EG, as is seen from the absorption spectra (black line in image D) and corresponding optical images (**E, F**).

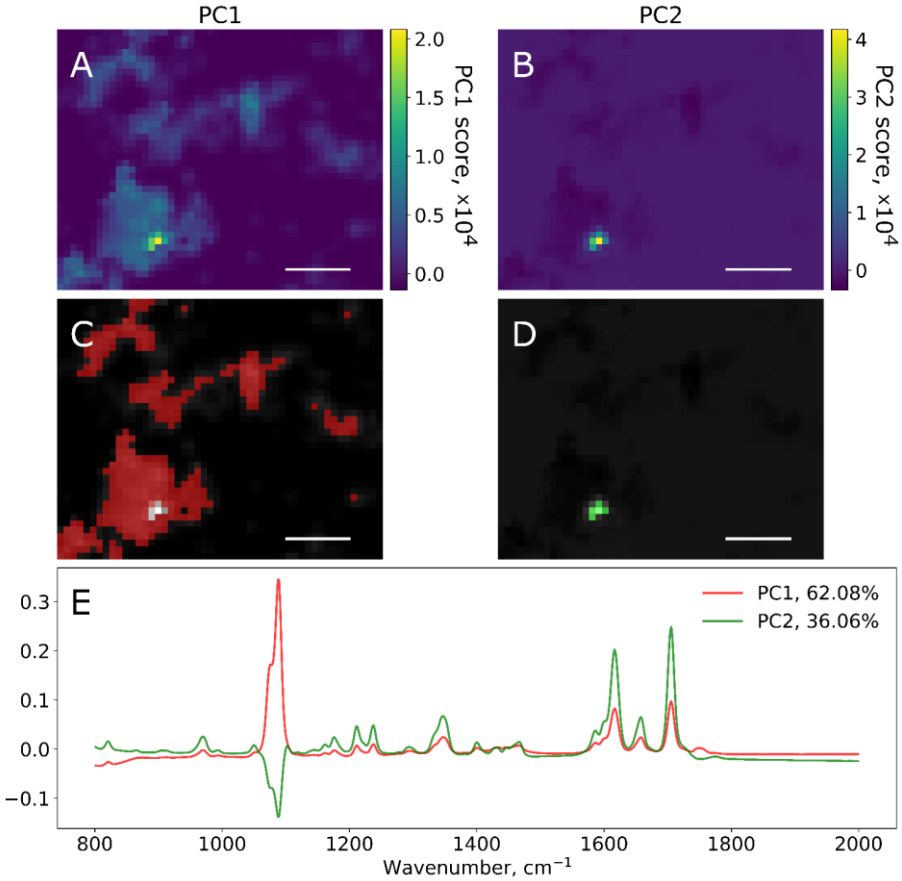

Figure SI 3. Raman mapping of Gf-loaded $CaCO_3$ carriers. **(A, C)** – 1st principal component (PC 1) and (**B, D**) – 2nd principal component (PC 2) in PCA decomposition score distributions. Red (C) and green (D) masks correspond to values (PC 1 and PC 2 scores, respectively) above thresholds calculated using Otsu's method. Spectra under the green mask were excluded from the red mask. The scale bars at (A-D) correspond to 10 μm. (E) PC 1 and PC 2 explaining 98.14% overall variance.

1st principal component (PC 1) of PCA decomposition showed the presence of vaterite contribution alongside with Gf impact on resulting Raman spectra (Figure SI 3 E). PC 2 demonstrated a more substantial Gf influence on the Raman signal with a negative vaterite contribution to it. Since the PCA provides a linear combination of the components' spectra with their coefficients at each data point, such a negative vaterite signal in PC 2 is necessary to compensate for the contribution of PC 1 to the Raman spectra. The first two components of PCA decomposition explained 98.14% overall variance. Otsu's threshold calculation method [47] was applied to distinguish signals from the background on the maps of the distributions of the PC 1 and PC 2 scores (Figure SI 3 C, D). Since PC 2 substantially impacted Raman spectra only in a small area under a green mask (Figure SI 3 D), we presumed that this area corresponded to griseofulvin crystal precipitated from the carriers during freeze-drying. By this means, the area under the red mask (Figure SI 3 C) corresponded to Gf-$CaCO_3$ carriers themselves indicating a fairly uniform distribution of the drug within the carriers.

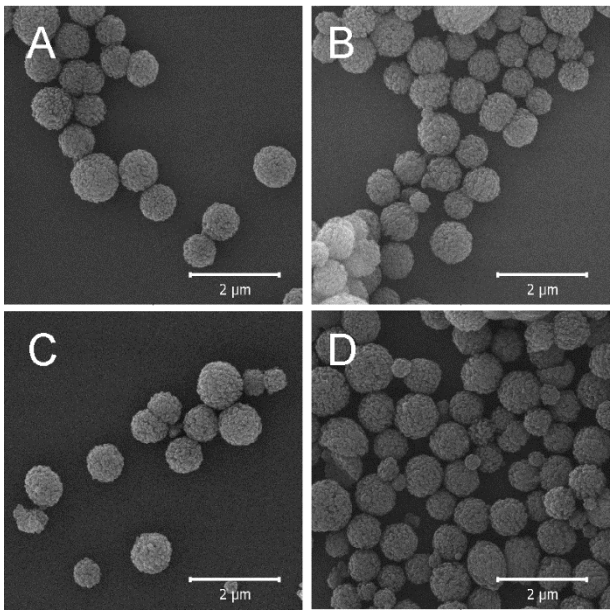

Figure SI 4. SEM images of griseofulvin-loaded vaterite carriers covered with various shell types: **A –** (Gf-$CaCO_3$)/HP, **B –** (Gf-$CaCO_3$)/PA/DS, **C** – (Gf-$CaCO_3$)/$(PA/DS)_2$, **D** - (Gf-$CaCO_3$)/$(PA/DS)_2$/HP.

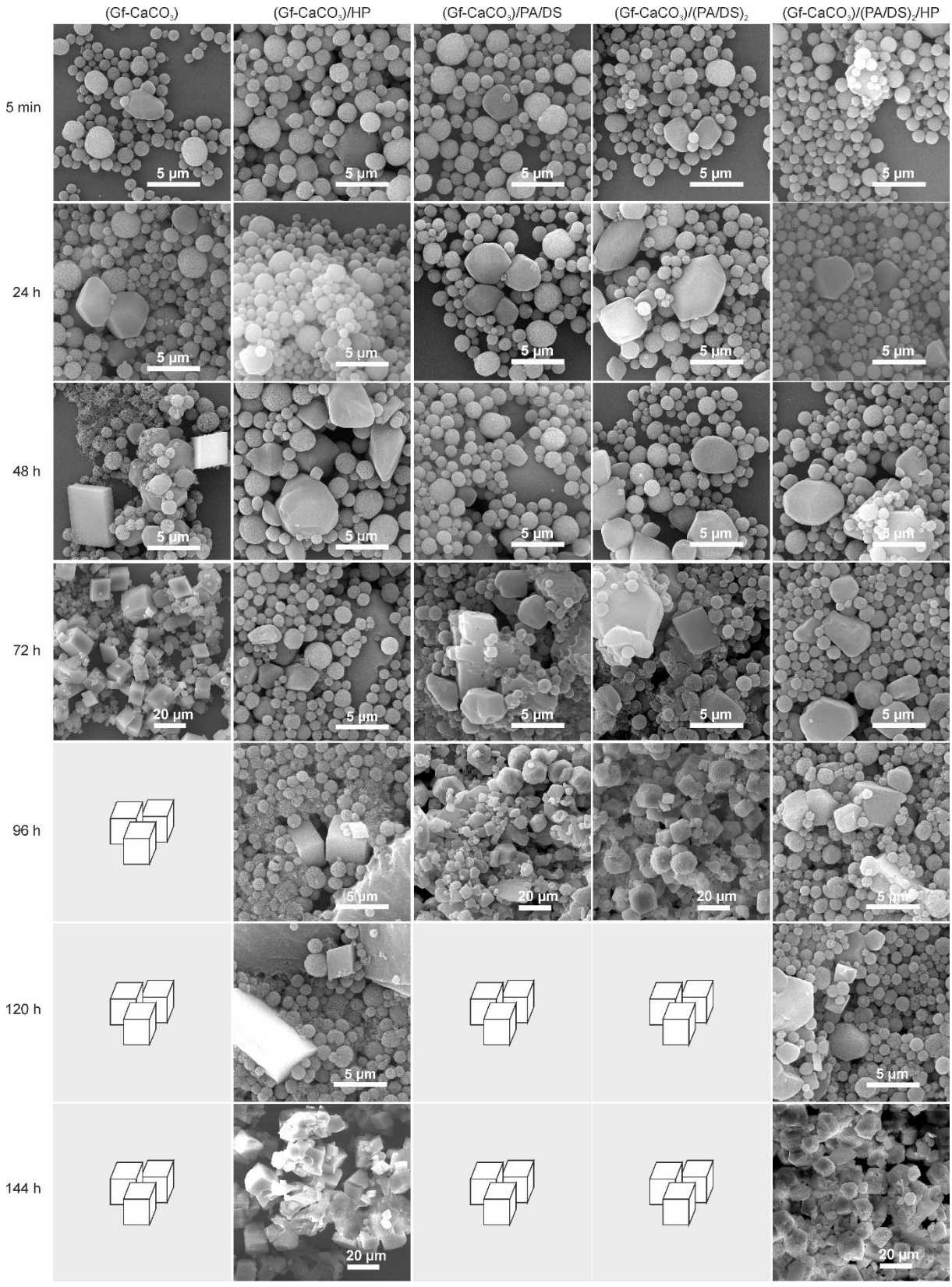

Figure SI 5. SEM images characterize the state of griseofulvin-loaded vaterite carriers covered with various types of PE shell in course of their incubation in deionized water (H_2O)

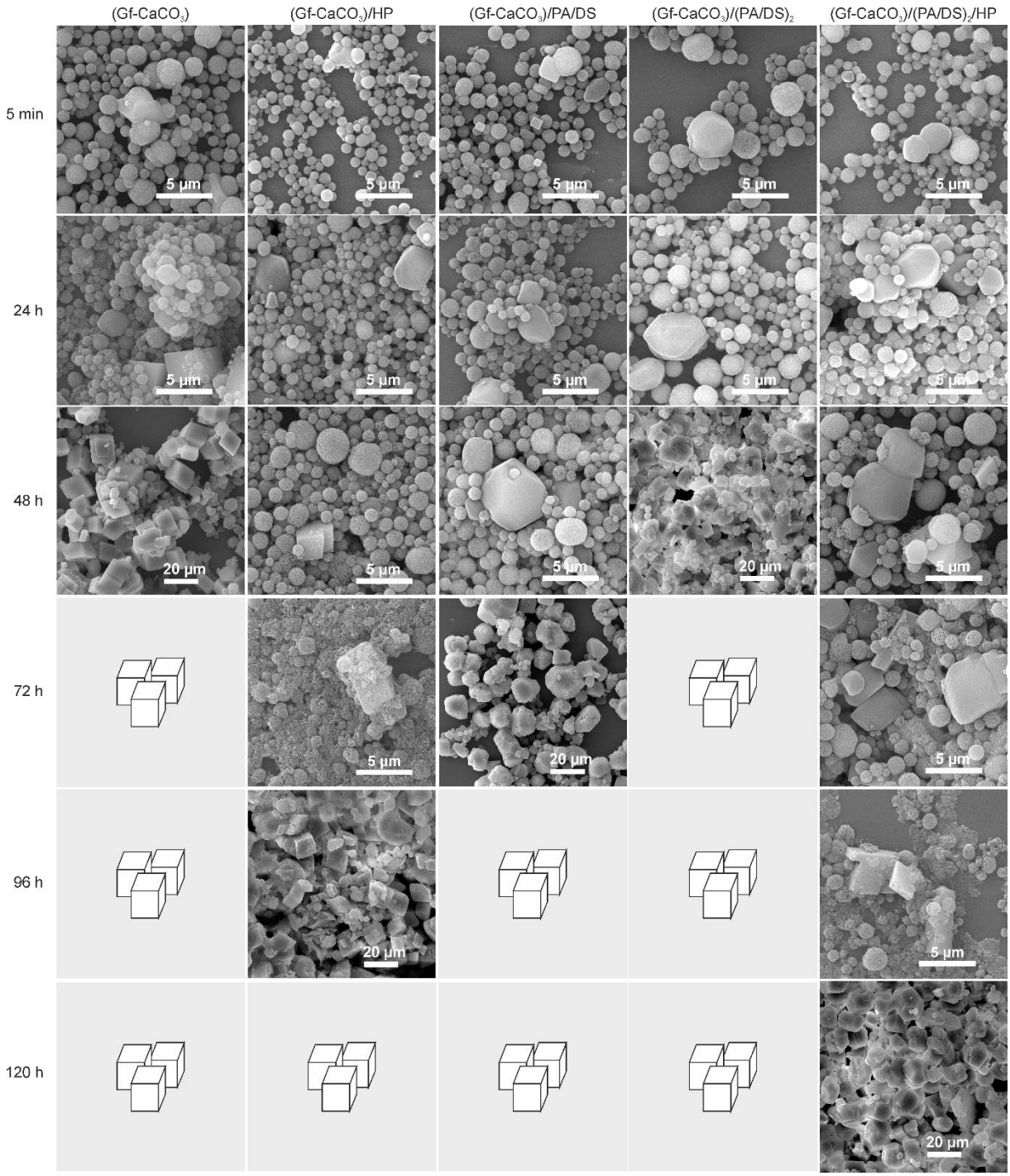

Figure SI 6. SEM images characterize the state of griseofulvin-loaded vaterite carriers covered with various types of PE shell in course of their incubation in saline (0.15M NaCl)

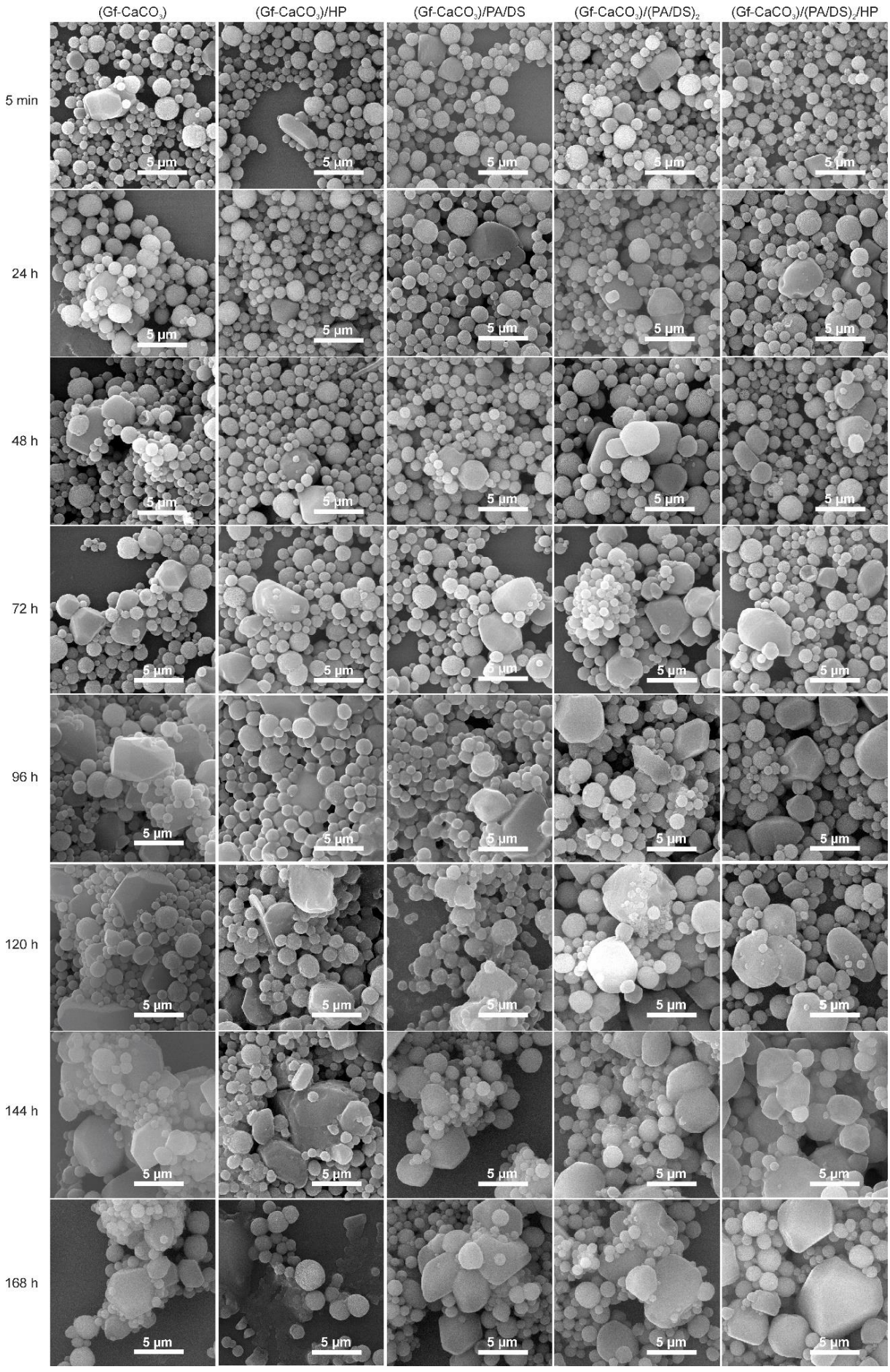

Figure SI 7. SEM images characterize the state of griseofulvin-loaded vaterite carriers covered with various types of PE shell in course of their incubation in cell cultural media (MEM)

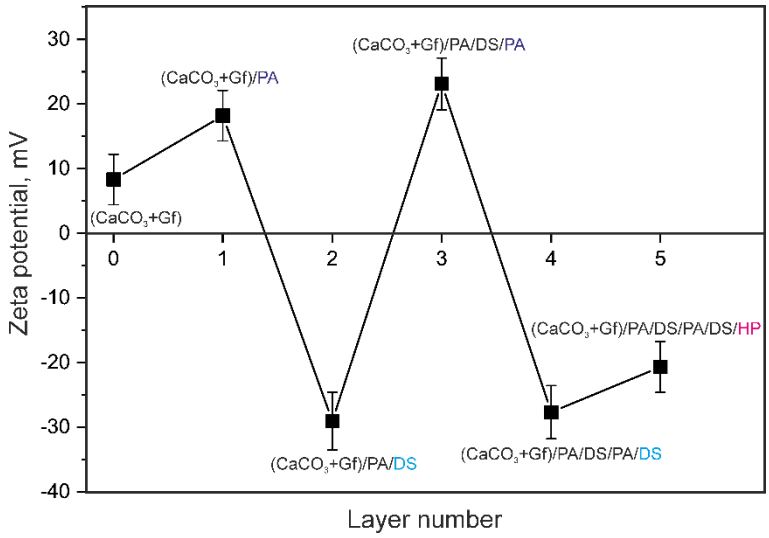

Figure SI 8. ζ-potential of griseofulvin-loaded vaterite carriers in course of polyelectrolyte (PE) shell formation: adsorption of poly-L-arginine hydrochloride (PA), dextran sulfate (DS) and heparin (HP) layers. The changes in the surface potential for Gf-loaded $CaCO_3$ particles registered after the deposition of each layer evidentiate the successful formation of the PE shell.

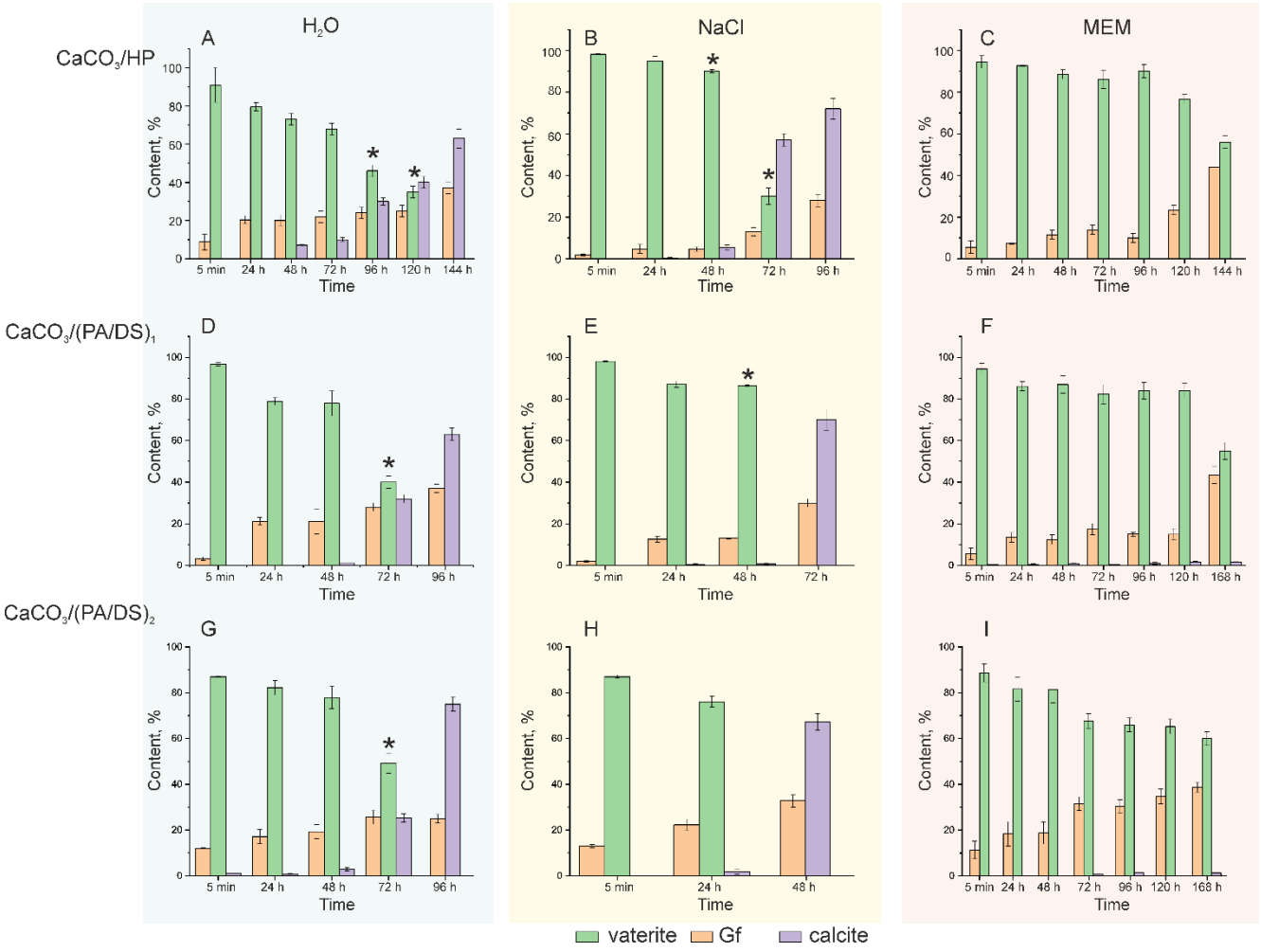

Figure SI 9. The diagrams representing the process of recrystallization of vaterite carriers loaded with griseofulvin (Gf) and covered with various shell types after their incubation in deionized water H_2O, saline 0.15 M NaCl and MEM. The asterisk * indicates the presence of the amorphous $CaCO_3$ phase in samples. The data are presented as a "mean value ± standard error".

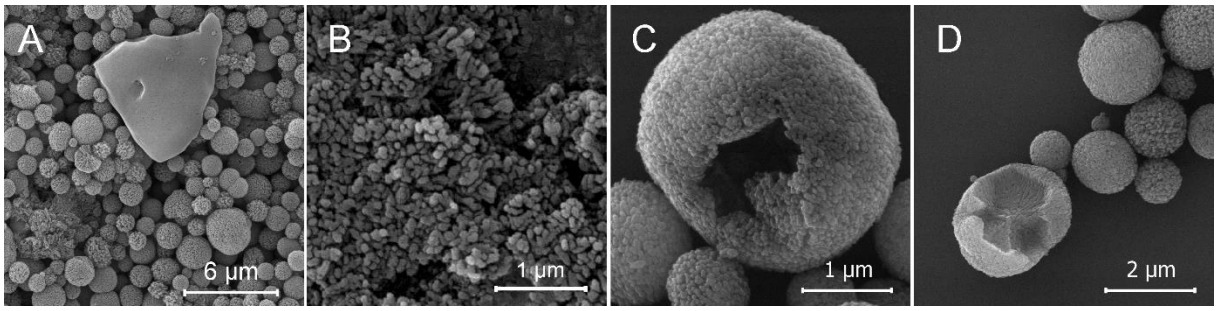

Figure SI 10. Characteristic SEM images illustrating the process of griseofulvin liberation from the (Gf-$CaCO_3$)/$(PA/DS)_2$/HP carriers during their incubation in deionized water: **A –** an overview image demonstrating the presence of integral and disrupted vaterite carriers, amorphous $CaCO_3$ phase and newly formed Gf particles; **B –** amorphous $CaCO_3$; **C** and **D –** disrupted and integral vaterite carriers

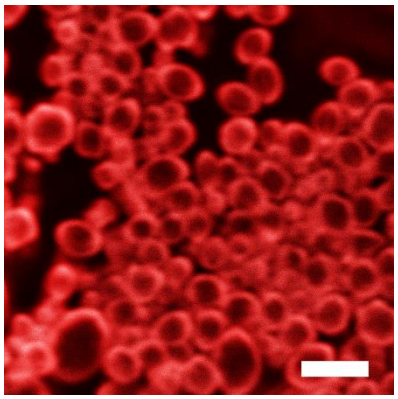

Figure SI 11. Characteristic CLSM image of griseofulvin-loaded vaterite carriers stained with rhodamine B fluorescent dye for the cellular uptake study. The scale bar corresponds to 2 μm

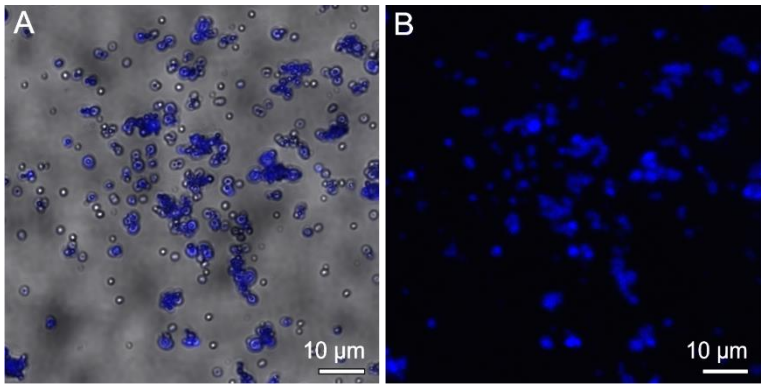

Figure SI 12. CLSM images of griseofulvin-loaded vaterite carriers (without any additional staining): (**A**) – overlay of the transmission and fluorescent images and (**B**) – fluorescent image. The blue fluorescence signal corresponds to the Gf drug successfully loaded into the carriers

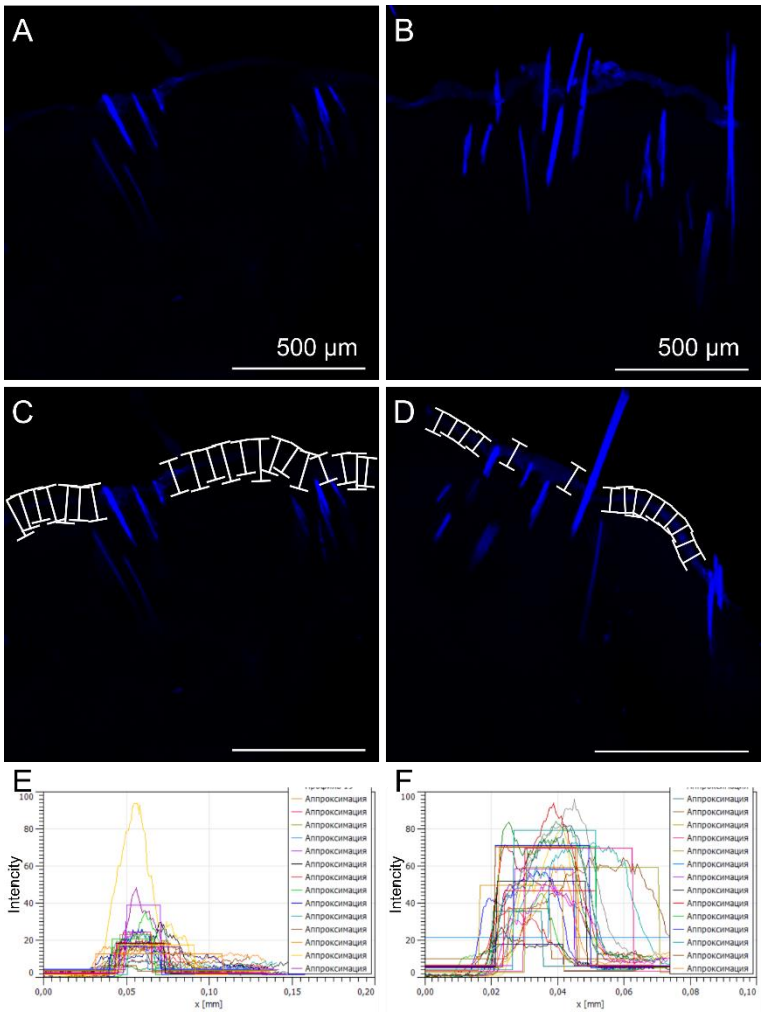

Figure SI 13. (**A-D**) – CLSM images of frozen rat skin slices demonstrating transdermal penetration of griseofulvin-loaded vaterite carriers *in vivo*; (**E, F**) – profiles of fluorescence intensity along the axes perpendicular to the skin surface (15-20 profiles for each of 3 cryoslices with averaging over 95 adjacent pixels): control skin samples from the site without carrier application (A, C, E) and skin samples after the carrier delivery (B, D, F)

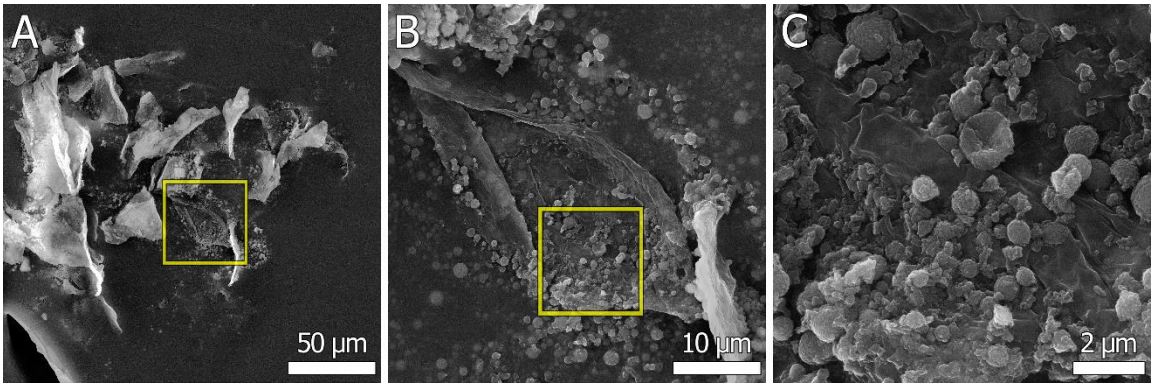

Figure SI 14. Penetration of Gf-loaded $CaCO_3$ carriers into hair follicles of rats *in vivo*. SEM images of the root sheath fragments of the hair plucked from the site of the carrier application. Images B and C represent the enlarged yellow-square marked areas of images A and B

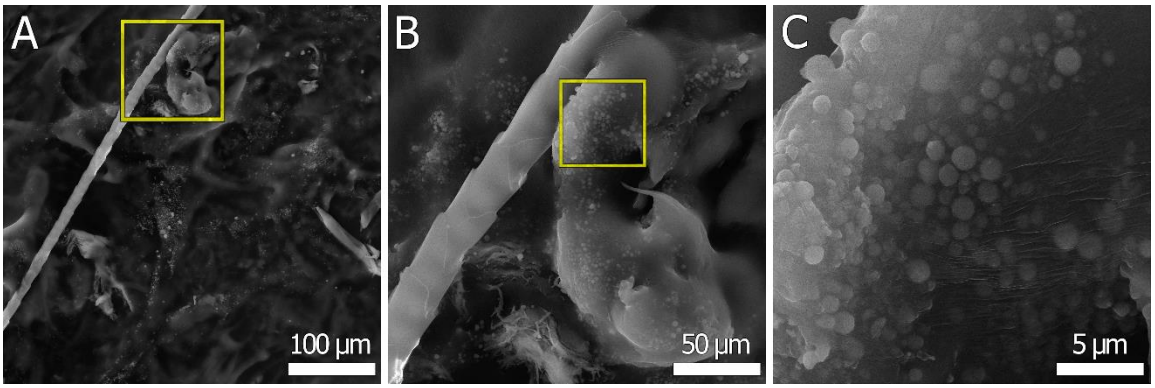

Figure SI 15. Penetration of the (Gf-$CaCO_3$)/$(PA/DS)_2$/HP carriers into hair follicles of rats *in vivo*. SEM images of the root sheath fragments of the hair plucked from the site of the carrier application. Images B and C represent the enlarged yellow-square marked areas of images A and B.

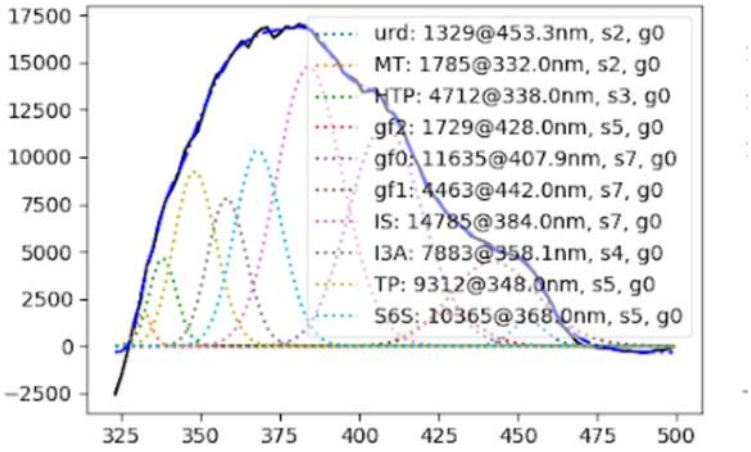

Figure SI 16. Typical control urine spectra with fitted peaks and resulting approximation curve

Table SI 1. Results of the statistical analysis for degradation dynamics of Gf-loaded $CaCO_3$ carriers of various structure in deionized water (Figure 4A). The indicated time points correspond to those, at which the differences in vaterite fraction between different carriers were statistically significant ($p<0.05$)

H_2O	(Gf-$CaCO_3$)	(Gf-$CaCO_3$)/HP	(Gf-$CaCO_3$)/PA/DS	(Gf-$CaCO_3$)/(PA/DS)$_2$	(Gf-$CaCO_3$)/(PA/DS)$_2$/HP
(Gf-$CaCO_3$)	•	•	•	•	•
(Gf-$CaCO_3$)/HP	48 h; 72 h; 96 h	•	•	•	•
(Gf-$CaCO_3$)/PA/DS	24 h; 48 h; 72 h	72 h; 96 h; 120 h	•	•	•
(Gf-$CaCO_3$)/(PA/DS)$_2$	5 min; 48 h; 72 h	72 h; 96 h; 120 h	5 min	•	•
(Gf-$CaCO_3$)/(PA/DS)$_2$/HP	48 h; 72 h; 96 h; 120 h	24 h; 48 h; 72 h; 96 h	24 h; 72 h; 96 h; 120 h	5 min; 48 h; 72 h; 96 h; 120 h	•

Table SI 2. Results of the statistical analysis for degradation dynamics of Gf-loaded $CaCO_3$ carriers of various structure in saline (Figure 4B). The indicated time points correspond to those, at which the differences in vaterite fraction between different carriers were statistically significant ($p<0.05$)

NaCl	(Gf-$CaCO_3$)	(Gf-$CaCO_3$)/HP	(Gf-$CaCO_3$)/PA/DS	(Gf-$CaCO_3$)/(PA/DS)$_2$	(Gf-$CaCO_3$)/(PA/DS)$_2$/HP
(Gf-$CaCO_3$)	•	•	•	•	•
(Gf-$CaCO_3$)/HP	24 h; 72 h	•	•	•	•
(Gf-$CaCO_3$)/PA/DS	24 h	72 h	•	•	•
(Gf-$CaCO_3$)/(PA/DS)$_2$	48 h	48 h; 72 h		•	•
(Gf-$CaCO_3$)/(PA/DS)$_2$/HP	72 h; 96 h	48 h; 72 h; 96 h	48 h; 72 h; 96 h	48 h; 72 h; 96 h	•

Table SI 3. Results of the statistical analysis for degradation dynamics of Gf-loaded $CaCO_3$ carriers of various structure in cell culture medium (Figure 4C). The indicated time points correspond to those, at which the differences in vaterite fraction between different carriers were statistically significant ($p<0.05$)

MEM	($Gf\text{-}CaCO_3$)	($Gf\text{-}CaCO_3$)/HP	($Gf\text{-}CaCO_3$)/PA/DS	($Gf\text{-}CaCO_3$)/$(PA/DS)_2$	($Gf\text{-}CaCO_3$)/$(PA/DS)_2$/HP
($Gf\text{-}CaCO_3$)	•	•	•	•	•
($Gf\text{-}CaCO_3$)/HP	96h; 120h; 144h; 196h	•	•	•	•
($Gf\text{-}CaCO_3$)/PA/DS	96h; 120h; 144h; 196h	24h	•	•	•
($Gf\text{-}CaCO_3$)/$(PA/DS)_2$	96h; 120h; 144h; 196h	24h; 96h	96h; 120h	•	•
($Gf\text{-}CaCO_3$)/$(PA/DS)_2$/HP	96h; 120h; 144h; 196h		96h; 120h		•